01 Jan 1990

A Study of the Hydration Properties of Selected Laser Dye Aerosols Including Continuous-Flow Parallel Plate and Alternating-Gradient Thermal Diffusion Cloud Chamber Measurements in the High Supersaturation Regime

Donald E. Hagen
Missouri University of Science and Technology, hagen@mst.edu

Max B. Trueblood
Missouri University of Science and Technology, trueblud@mst.edu

Darryl J. Alofs
Missouri University of Science and Technology, dalofs@mst.edu

Recommended Citation

D. E. Hagen et al., "A Study of the Hydration Properties of Selected Laser Dye Aerosols Including Continuous-Flow Parallel Plate and Alternating-Gradient Thermal Diffusion Cloud Chamber Measurements in the High Supersaturation Regime," *Aerosol Science and Technology*, vol. 12, no. 3, pp. 547 - 560, Taylor and Francis Group; Taylor and Francis, Jan 1990.
The definitive version is available at https://doi.org/10.1080/02786829008959369

Aerosol Science and Technology

ISSN: 0278-6826 (Print) 1521-7388 (Online) Journal homepage: https://www.tandfonline.com/loi/uast20

A Study of the Hydration Properties of Selected Laser Dye Aerosols Including Continuous-Flow Parallel Plate and Alternating-Gradient Thermal Diffusion Cloud Chamber Measurements in the High Supersaturation Regime

Donald E. Hagen , Max B. Trueblood & Daryl J. Alofs

To cite this article: Donald E. Hagen , Max B. Trueblood & Daryl J. Alofs (1990) A Study of the Hydration Properties of Selected Laser Dye Aerosols Including Continuous-Flow Parallel Plate and Alternating-Gradient Thermal Diffusion Cloud Chamber Measurements in the High Supersaturation Regime, Aerosol Science and Technology, 12:3, 547-560, DOI: 10.1080/02786829008959369

To link to this article: https://doi.org/10.1080/02786829008959369

Published online: 08 Jun 2007.

A Study of the Hydration Properties of Selected Laser Dye Aerosols Including Continuous-Flow Parallel Plate and Alternating-Gradient Thermal Diffusion Cloud Chamber Measurements in the High Supersaturation Regime

Donald E. Hagen,* Max B. Trueblood, and Daryl J. Alofs†
Graduate Center for Cloud Physics Research, University of Missouri-Rolla, Rolla, MO 65401

The hydration behavior of aerosols, made up of various fluorescent dyes, when exposed to water saturation or supersaturated conditions has been studied. Critical supersaturation spectra are reported. The dyes are found to behave as high molecular weight ionic compounds that obey Kohler theory. Their relevant Kohler parameters are measured. This study makes use of and compares results from the isothermal haze, continuous-flow, and alternating-gradient thermal diffusion cloud chambers. The ability of the continuous-flow thermal diffusion chamber to operate correctly at high supersaturations is shown.

INTRODUCTION

The study of fluorescent laser dye properties is a broad and interesting subject. Most of the existing knowledge about these dyes concerns their properties as a solute in a suitable solvent. However, as their range of applications broadens, their properties as aerosols have become important. Fluorescent dyes are used as tracers for air parcels in atmospheric field experiments, e.g., in the airborne lidar experiments of Uthe and coworkers (Uthe et al., 1985). In laboratory work fluorescent dyes have been used for precision droplet sizing (Tzeng et al., 1983). In particular, the hygroscopic behavior of fluorescent dyes is an important property. When dispersed in aerosol form, a dye particle's hygroscopicity will influence its water content and therefore its mass, its ability to follow a moving air parcel, its probability of being scavenged, its fluorescence capabilities, and whether or not it precipitates out.

Our laboratory is preparing an aerosol scavenging experiment for our cloud simulation facility (White et al., 1987) that will employ fluorescent laser dye aerosols. This provided the motivation for a study of the hydration behavior of these dye aerosols. This study covers a broad range of fluorescent dye materials, supersaturations to which the aerosols are exposed, and dye particle sizes. The results, cast into the form of critical supersaturation (SS_C) information for a given dry particle diameter (D_p) and material, are reported here.

Several diffusion cloud chamber instruments were used in the study to determine critical supersaturation since a broad range of supersaturation conditions was covered. These included the isothermal haze chamber (IT), the continuous-flow thermal diffusion chamber (CFD), and the alternating-gradient thermal diffusion chamber (ALGR). Each instrument covered a certain

*Also of the Department of Physics.
†Also of the Department of Mechanical and Aerospace Engineering.

Aerosol Science and Technology 12:547–560 (1990)

0278–6826/90/$3.50

subrange of the total range of supersaturations.

An important facet of this study is the validation of instrument performance. This study constitutes the first verification that the supersaturations produced in the ALGR are near to the expected values. This study also constitutes the first performance verification of the supersaturations produced in the CFD at supersaturations greater than 1%.

These two verifications were accomplished by 1) studying the aerosol behavior in a supersaturation region where the CFD performance is well known and trusted, thereby developing a knowledge of the aerosol's hygroscopic behavior, 2) extrapolating this behavior with theory to predict the relation between SS_C and D_p at higher SS_C, and 3) then experimentally verifying that this predicted behavior agrees with the instruments' observations.

APPARATUS

The task of studying the hydration properties of fluorescent dye aerosols involves the use of several pieces of apparatus. Figure 1 shows that the experimental apparatus consisted of a Collison nebulizer (CN) to produce an aerosol, a differential mobility analyzer (DMA) to remove from the aerosol stream all particle sizes other than the one size being studied at that time, cloud chambers (CFD/IT and ALGR) to expose the aerosol to the desired supersaturation and temperature, and optical particle counters (OPC) to sense and record whether or not the aerosol activated (passed over the energy barrier and became a freely growing water droplet) under those conditions.

A tank of either compressed nitrogen or compressed breathing air drove the nebulizer. The nebulizer used was the fluid atomization aerosol generator (model 7300, Environmental Research Corp., St Paul,

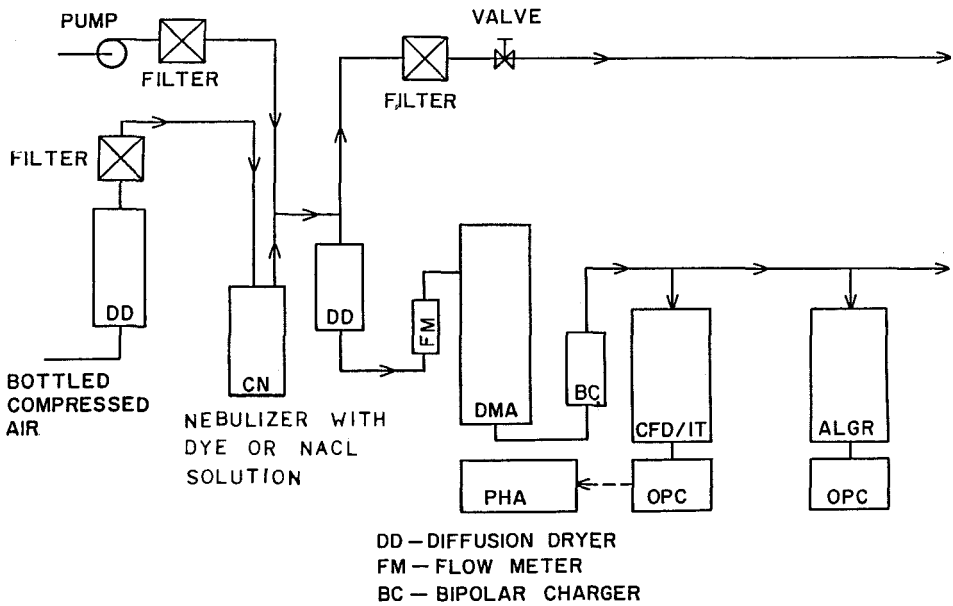

FIGURE 1. Apparatus block diagram.

MN), which is a three-jet, stainless steel, Collison type (May 1972) atomizer.

It is essential that the aerosol particles be nearly dry when they pass through the DMA in order that D_p be accurately known. Thus the diffusion dryers (DD) are present (Figure 1) in order to reduce the relative humidity to about 20%. The diffusion dryers consist of cylindrical layers, the outermost being a casing, to withstand the slightly positive line pressure without leaking, the next layer being granules of a desiccant material, and the innermost layer being a metal screen, to hold the desiccant in place. The aerosol sample flows through the tube formed by the screen; thus by molecular diffusion, water vapor passes from the aerosol into the desiccant material. The length and diameter of the cylindrical screen are 60 cm by 1.2 cm, respectively, and the air flow rate through the dryer was 0.6 L/min.

The differential mobility analyzer (DMA) was developed by Liu and Pui (1974a, 1974b) and by Knutsen and Whitby (1975a) and is commercially available (model 3071, Thermo-Systems, Inc., St. Paul, MN). Its function is to pass only aerosol particles in a narrow electric mobility range. For singly charged particles this leads to an output aerosol that is monodispersed in size.

All the particles in the monodisperse aerosol output Q_M of the DMA are positively charged. To avoid losses through undesirable electrostatic effects, the aerosol is then neutralized (brought to a Boltzmann equilibrium charge distribution) by passing it near a radioactive source, also called a bipolar charger (BC). The bipolar charger used is one that is commercially available (model 3077, Thermo-Systems, Inc.).

A small flow (8 cm^3/min) of aerosol passed into the CFD/IT. The CFD/IT is a dual-mode cloud chamber that measures the SS_C of a condensation nucleus (Alofs, 1978; Alofs et al., 1979; Alofs and Trueblood, 1981). A thorough description of its operation and performance is provided in the references above and more description will be provided later in this paper.

Another small portion of the aerosol flow (10 cm^3/min) passed into the ALGR, which is another type of continuous-flow thermal diffusion cloud chamber (Hoppel et al., 1979a, b).

PREPARATION OF AEROSOLS

Several highly pure fluorescent laser dyes (marketed as the lasing agent for dye lasers) were selected on the basis of their being somewhat soluble in water and the fact that they are excited to fluorescence by the 488-nm line of the argon ion laser. The laser dyes were purchased from Exciton (Dayton, OH), except for the sulforhodamine B, which came from Eastman Kodak Co. (Rochester, NY). The rhodamine 590 chloride (also called rhodamine 6G) is a recognized carcinogen. The disodium fluorescein is also called uranine and Drug and Cosmetic Yellow No. 8. Since all the dyes were very pure as delivered, no attempt was made to purify them.

A very dilute solution of a dye was prepared and then nebulized. The water for the nebulizer was doubly distilled and typically had a specific resistance of 0.275 MΩ. The water in the resultant drops evaporated, leaving behind dry, airborne dye particles.

Considerable care was taken to ensure that the dye solutions remained pure and uncontaminated. The nebulizer jar and nebulizer jet head were rinsed about 15 times with punctilious ethanol and doubly distilled water before the new dye solution was poured into it. Even after this amount of precaution was taken, sometimes the first dye solution gave results inconsistent with later dye solutions. The data reported in this paper are the result of experiments done with at least four separate dye solutions for each dye.

MEASUREMENTS OF THE CRITICAL SUPERSATURATION USING THE ISOTHERMAL CHAMBER

The CFD/IT chamber (Figure 2) is composed of two parallel plates (one warm and one cool) 100 cm long, 13 cm wide, and separated by about 0.8 cm. The plate surfaces facing one another are covered with filter paper which is continuously saturated with doubly distilled water. The aerosol is metered into the CFD/IT at the top through a 0.25-mm ID tube and remains in a narrow, coherent stream all the way to a 1.3-mm ID tube which is centered between the two plates at the downstream end of the chamber. Water droplets formed on the aerosol particles travel through this 1.3-mm ID tube to the OPC, where they are counted and/or sized.

For nuclei with SS_C between 0.0133% and 0.173%, the CFD/IT is operated in the isothermal mode. Here the warm plate, cool plate, and optical particle counter (OPC) are all thermostated at 25.0°C. Thus the nuclei are exposed to a relative humidity of 100%. Although the nuclei do not activate, they do take on water and grow to an equilibrium diameter, D_{100}. This D_{100} of the aerosol particle is related to its SS_C by the Laktionov relation (Alofs and Podzimek, 1974; Laktionov, 1972),

$$SS_C = 0.08/D_{100}, \quad (1)$$

where SS_C is in percent and D_{100} is in micrometers. Note that this relation is insensitive to the chemical nature of the particle even though both SS_C and D_{100} depend on composition. Hence a measure of D_{100} yields the particle's SS_C.

The response of the OPC (a voltage pulse) as a droplet passes through its sensitive volume is a function of the size of the particle or droplet. It is also a function of the index of refraction of the droplet or particle. The voltage pulses from the OPC are the input to a pulse height analyzer (PHA). The PHA is model 220, Nuclear Data, Inc., Schaumburg, IL. The relation between SS_C and a particular channel of the PHA is determined by calibration with monodisperse NaCl aerosol particles (Alofs and Trueblood, 1981). The calibration procedure was to nebulize an NaCl solution, select a monodisperse aerosol of diameter D_p, grow water drops of equilibrium diameter D_{100} in the IT, and categorize (according to pulse height) the OPC pulses in the PHA. Since the Kohler theory allows calculation of the SS_C of the NaCl nuclei of diameter D_p (which is known from the DMA setting), a calibration point of the IT/OPC (SS_C vs. channel with the most pulses) is thereby obtained. This procedure was repeated for different sizes to arrive at a complete calibration curve.

Then the NaCl solution was replaced with a laser dye solution and the SS_C of the monodisperse dye aerosol of diameter D_p was determined from the calibration curve. Results (critical supersaturation SS_C vs. particle diameter D_p) of these experiments are labeled as IT points in Figures 3–6.

FIGURE 2. Continuous flow thermal diffusion/isothermal haze cloud chamber diagram.

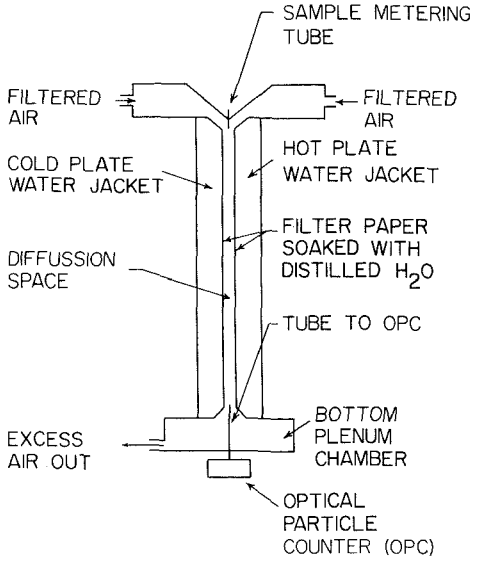

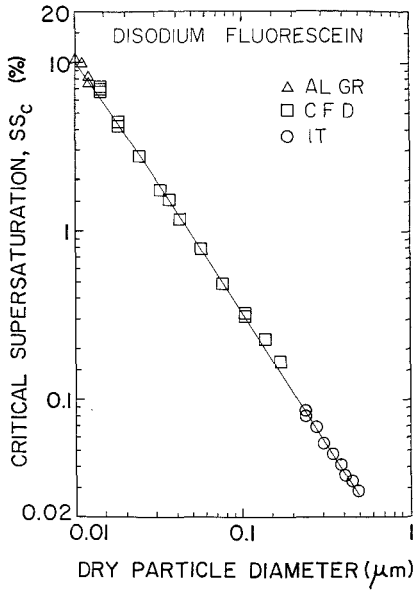

FIGURE 3. Critical supersaturation vs. particle diameter for disodium fluorescein. (Δ) ALGR (alternating-gradient chamber) data; (□) CFD (continuous-flow thermal diffusion chamber) data; (○) IT (isothermal haze chamber) data; (—) Kohler theory.

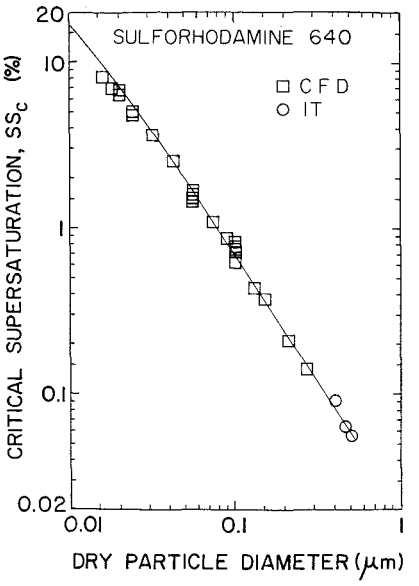

FIGURE 5. Critical supersaturation vs. particle diameter for sulforhodamine 640. (□) CFD data; (○) IT data; (—) Kohler theory.

FIGURE 4. Critical supersaturation vs. particle diameter for rhodamine 590 chloride. (Δ) ALGR data; (□) CFD data; (○) IT data; (—) Kohler theory.

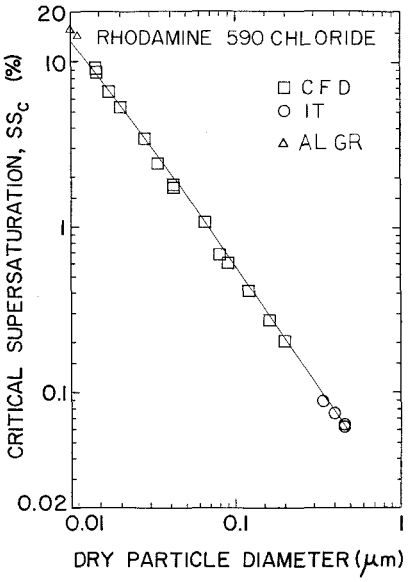

FIGURE 6. Critical supersaturation vs. particle diameter for sulforhodamine B. (□) CFD data; (○) IT data; (—) Kohler theory.

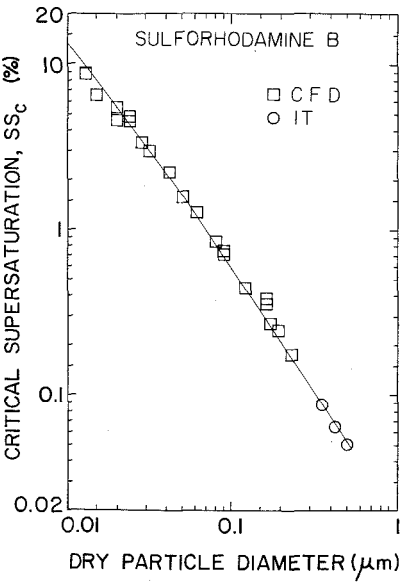

MEASUREMENTS OF THE CRITICAL SUPERSATURATION USING THE CONTINUOUS-FLOW DIFFUSION CHAMBER, $SS_C < 1.0\%$

For nuclei with an SS_C between 0.10% and 9.0%, the CFD/IT is operated in the CFD mode (Alofs et al., 1979). Here the warm plate and the OPC are thermostated at $T_H = 25.0°C$. The cool plate is thermostated at some adjustable lower temperature T_C. As the air flow passes through the chamber, equilibrium profiles of gas temperature and water vapor pressure develop downstream, such that temperature and vapor pressure are linear functions of position between the plates. The equilibrium water vapor pressure is approximately a parabolic function of temperature, however, and so a supersaturation develops with the peak value SS_{CFD} being halfway between the plates.

The residence time of the sample in the chamber is sufficient that nuclei with an $SS_C < SS_{CFD}$ will activate, producing water

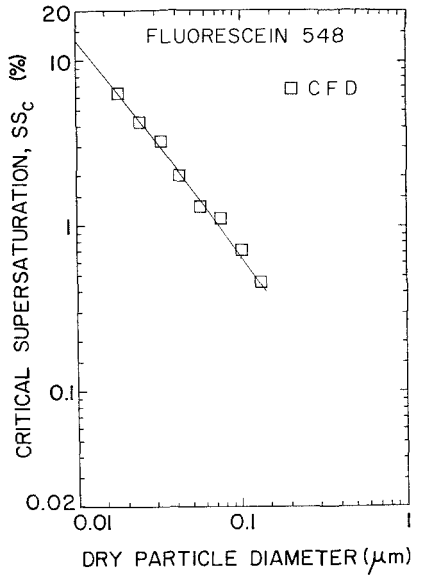

FIGURE 8. Critical supersaturation vs. particle diameter for fluorescein 548. (▣) CFD data; (—) Kohler theory.

FIGURE 7. Ratio of aerosol concentrations as measured by the CFD and the ALGR chambers vs. CFD operating supersaturation for the residence time experiment.

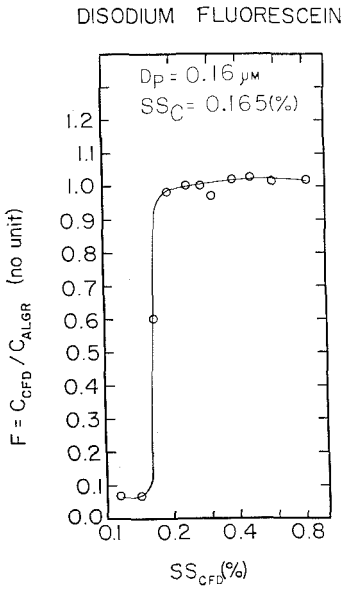

FIGURE 9. Critical supersaturation vs. particle diameter for rhodamine 560 chloride. (Δ) ALGR data; (□) CFD data; (—) Kohler theory.

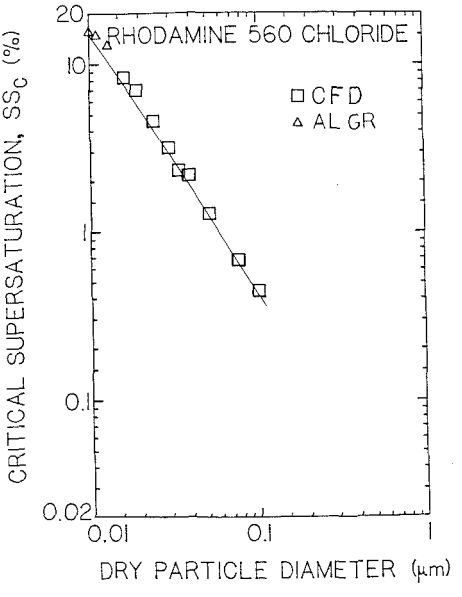

drops of several microns in diameter, which are then large enough to be counted by the OPC. The temperature, T_C, of the cold plate is increased in a stepwise manner (lowering SS_{CFD}). The ratio $F = C_{CFD}/C_{ALGR}$ (where C_{CFD} and C_{ALGR} are the concentrations as measured by the CFD and ALGR, respectively) is plotted vs. SS_{CFD}. The SS_C is chosen as that value of SS_{CFD} for which $F = 0.5$. By normalizing C_{CFD} with C_{ALGR}, one prevents any temporal fluctuations in the nebulizer output from affecting the results. A typical such curve for disodium fluorescein is shown in Figure 7. This experiment was repeated for many different D_p settings of the DMA. Results of this type of experiment for the six laser dyes are shown in Figures 3–6 and 8 and 9.

MEASUREMENTS OF THE CRITICAL SUPERSATURATION USING THE CONTINUOUS-FLOW DIFFUSION CHAMBER, $SS_C \geq 1.0\%$

In previous work with the CFD, Alofs (1978) only claimed that it was valid up to 1% supersaturation. Higher supersaturations were not attempted at that time primarily because they were not of interest, i.e., they rarely occur in natural air masses (Carstens, 1979; Davies, 1987). The present CFD, with downward vertical air flow between vertical plates can operate at supersaturations greater than 1%, but one must take measures to avoid several potential problems.

The first potential problem involves the free convection cell caused by the vertical surfaces of the hot and cold plates (Sinnarwalla and Alofs, 1973; Alofs, 1978). Because of the vertical orientation of the plates, there is an upward buoyancy near the hot plate, and a tendency for backflow there. If this superimposed free convection cell becomes comparable to the forced convection field, then the crossover region in the bottom plenum chamber may move up out the plenum chamber and cause some of the drops to be recirculated. Also, transient supersaturations occur in the bottom crossover region (Saxena and Carstens, 1971). These problems can be circumvented by maintaining a sufficiently high forced convection. Sinnarwalla and Alofs (1973) give an expression for the minimum value of the air flow rate (Q_F) needed to insure this condition.

A second restriction at high SS_{CFD} is that the flow rate must be sufficiently large that the drops do not grow so large that they impact at the entrance to the 1.3-mm ID tube at the bottom. Impacted drops accumulate to form a huge drop that runs down the inside of this tube, makes its way to the OPC-sensitive volume and causes spurious signals in the OPC. Experiments with the CFD using a monodisperse aerosol (with a stable output concentration), whereby one measures the apparent concentration as a function of time, with droplet diameter as a parameter, show that the maximum allowable droplet diameter to avoid this unwanted impaction is 25 μm.

This restriction on droplet diameter imposes a constraint on the time that the droplet spends in the CFD, hereafter called the flight time (t_F), and hence also places a constraint on the air flow rate. Comparing the restrictions on the air flow due to droplet impaction to the restrictions required to avoid free convection backflow reveals that the former consideration is more stringent than the latter. The last column in Table 1 is the recommended flight time (t_F) in the chamber for monodisperse aerosols (with

TABLE 1. Characteristic Times vs. Supersaturation in Continuous-Flow Diffusion Chamber CFD

SS_{CFD} (%)	t_p (s)	t_R (s)	t_G (s)	t_F (s)
0.7	41.8	1.39	1.60	14.0
1.0	35.0	1.34	1.25	8.33
3.0	20.2	1.18	0.69	6.33
7.0	13.2	1.07	0.62	5.00
10.0	1.1	1.03	0.52	4.33

SS_C: $0.75SS_{CFD} < SS_C < SS_{CFD}$) such that the droplets formed on them do not impact at the 1.3-mm tube.

The third potential problem involves the diffusiophoretic and thermophoretic forces, both of which push the aerosol stream away from the region of peak supersaturation (midway between the plates) and toward the cool plate. Sinnarwalla and Alofs (1973) give an expression for the maximum allowable residence time due to phoretic displacement (t_p), with t_p defined such that the nuclei stay in the region where the supersaturation is $\geq 0.9SS_{CFD}$. Table 1 shows values of t_p for $0.7\% \geq SS_{CFD} \geq 10\%$. A discussion of these values will be deferred until later so that connections can be made with other potential problems. A related concern is that the optimum position (between the CFD plates) of the aerosol injection needle may vary with SS_{CFD}. The position of this needle is set by a permanently mounted translation table. The optimum needle position was found to be insensitive to SS_{CFD} in the supersaturation range 0.3% to 4.1%.

The fourth potential problem in going to the region $SS_{CFD} \geq 1\%$ is the concern that at large flow rates the supersaturation profile between the hot and cold plates might not be fully developed in an air parcel traveling down between the plates by the time that air parcel arrived at the 1.3-mm tube. Let the rise time (t_R) be defined as the time needed for the supersaturation at the midplane to develop to $0.9SS_{CFD}$. An approximate expression for t_R was derived by Mahata et al. (1973). Table 1 lists values of t_R as a function of SS_{CFD}.

A fifth consideration is the growth time needed to grow a detectable droplet. A numerical cloud model (Hagen, 1979) was used to determine the growth time, t_G, defined as the time required for a dry aerosol particle with an $SS_C = 0.9SS_{CFD}$ to take on water and grow to an easily detectable droplet, here taken to be a droplet of 2.0-μm diameter. Table 1 also lists these t_G values. These calculations were performed for supersaturation histories close to those occurring in the CFD.

Table 1 shows that 1) the flight time, t_F, is always considerably less than the t_P, the maximum allowable flight time due to phoretic considerations, 2) the rise time t_R is always considerably less than the flight time t_F, and 3) the growth time t_G is always considerably less than the flight time t_F. Thus the CFD can be operated in such a way that the above problems can be satisfactorily avoided.

A sixth potential difficulty at high supersaturations concerns the possibility that aerosols with widely different critical supersaturations may be introduced into the CFD. This difficulty does not arise in our present fluorescent aerosol experiment involving monodisperse aerosols composed of a single clearly defined chemical species, but could arise in a more general case, e.g., 1) one involving an aerosol monodispersed in size but composed of different chemical species, or 2) a polydispersed aerosol composed of a single chemical. At high operating supersaturation the supersaturation profile takes relatively long to develop. Aerosols with different critical supersaturations will activate at different points along the trajectory as the supersaturation develops. They will then have different amounts of time for growth and will differ in final size at the CFD exit port. As a consequence those particles with a low SS_C would activate first and possibly grow sufficiently large to cause vapor depletion and interfered with the activation of high SS_C particles, thereby causing them to be uncounted. Alternately, relatively large low SS_C particles might be lost through impaction, and thereby be missed in the counting.

This problem can be analyzed using droplet growth theory to explicitly track the evolution of the different drop classes. Theoretical calculations were done for aerosols with critical supersaturations equal to 10% and 90% of that present in the CFD, and these show that droplets formed on aerosol

particles with radically different SS_C produce droplets of almost equal size after sufficient growth time (approximating that used in the CFD) is allowed.

Table 2 summarizes the results of these calculations. The left most column shows the terminal supersaturation, SS_{CFD}. The next column is the flight time, t_F, in the CFD. Next is the diameter, $d_{0.1}$, of the droplet formed on an aerosol particle with SS_C equal to one-tenth the applied supersaturation, SS_{CFD}. The last column is the diameter, $d_{0.9}$, of the droplet formed on a nucleus with SS_C equal to nine-tenths the applied supersaturation, SS_{CFD}. Clearly the droplets formed on these two radically different nuclei are practically indistinguishable. Hence the CFD can be used to measure the concentration vs. critical supersaturation spectrum, even at high supersaturation, for aerosols containing a mixture of critical supersaturations.

The above discussion indicates that the problems anticipated with CFD operations at high supersaturations can be overcome. The final proof, however, must lie within an experiment. Such an experimental test is the measurement of the critical supersaturation spectrum of a material whose spectrum is well known, e.g., NaCl. Alofs et al. (1979), and Gerber et al. (1977) in their studies of NaCl aerosols have shown that NaCl aerosols accurately follow the critical supersaturation profile given by Kohler theory (Hanel, 1976), for supersaturation ratios $S < 1\%$. Here we measure the critical supersaturation profile for $S > 1\%$ and show that it agrees with that given by Kohler theory.

TABLE 2. Droplet Diameter for Two Classes of Aerosol Particles

SS_{CFD} (%)	t_F (s)	$d_{0.1}$ (μm)	$d_{0.9}$ (μm)
10	4.36	20.2	19.7
7	5.0	18.5	18.18
3	6.2	13.5	13.3
1	8.1	8.96	8.7
0.7	14.1	10.0	9.68

NaCl aerosols were generated using the Collison nebulizer/DMA technique and their critical supersaturations measured. Results of these experiments are shown in Figure 10. The CFD is found to operate properly in this supersaturation regime. The experimental values for SS_C agree with the theoretical values from the Kohler equations up to about 4.5%. Higher values of SS_C were not attempted because of the difficulty in operating the DMA at $D_p < 0.01$ μm.

Later sections of this paper report measurements of SS_C spectra for various fluorescent dyes over a broad range of supersaturation. Continuity of the CFD data for $S > 1\%$ with that from the CFD at $S < 1\%$, along with that from other chambers, and with Kohler theory give further evidence that the CFD is working properly in the $S > 1\%$ regime.

FIGURE 10. Critical supersaturation vs. particle diameter for NaCl aerosols. (□) NaCl experiment; (—) Kohler theory.

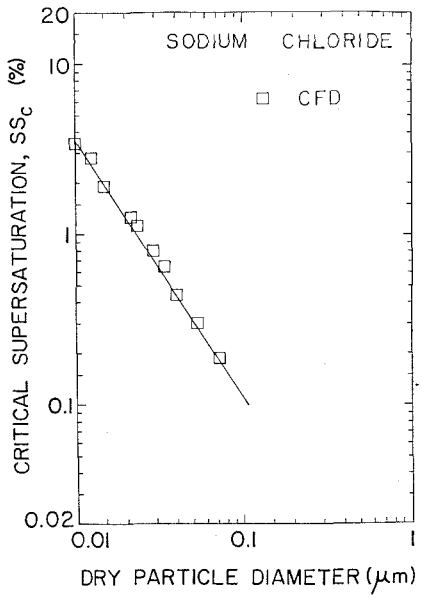

MEASUREMENTS OF THE CRITICAL SUPERSATURATION USING THE ALTERNATING-GRADIENT CHAMBER

A few experiments were done to measure the SS_C of disodium fluorescein, rhodamine 560 chloride, and rhodamine 590 chloride using the ALGR. Here the supersaturation (SS_{ALGR}) imposed by the alternating-gradient chamber was lowered until the concentration (C_{ALGR}) as measured by the ALGR fell to half the steady-state value and that value of SS_{ALGR} was taken as the SS_C.

There are several potential problems inherent in using the ALGR for such temperature sweeps. First, one must rely on the nebulizer output being fairly constant here because temporal fluctuations in the nebulizer output cannot be eliminated by normalization with a reference instrument.

The second problem involves the natural, inherent fluctuations in SS_{ALGR} along the axis. The amplitude of these SS_{ALGR} fluctuations are determined by the filtered air flow rate Q_F, as can be seen by inspecting Figure 2 of Hoppel et al. (1979b). By keeping the flow rate at or near the value given by Hoppel et al. one minimizes the effects of these fluctuations.

The SS_C vs. size data taken for these three dyes with the ALGR chamber are shown in Figures 3 (disodium fluorescein), 4 (rhodamine 590 chloride), and 9 (rhodamine 560 chloride). This data shows good continuity with the CFD data in the overlap regions of these two instruments.

KOHLER THEORY

The classical theory for hygroscopic behavior of aerosol particles was developed by Kohler (1921a, b, 1922, 1927, 1936). Pruppacher and Klett (1978) provide the following relation for the equilibrium droplet radius (a) of a solution droplet in an ambient supersaturation SS:

$$SS = A/a - BQ/(a^3 - r^3), \tag{2}$$

where

$$A = 2\,M_w\sigma/(RT\rho_w),$$

$$B = M_w D_p^3/8\rho_w M_s,$$

$$Q = \nu\phi_s\rho_s$$

$$r = 0.5D_p(\rho_s/\rho_w)^{0.333},$$

M_w is the molecular weight of water, σ is the surface tension of water with respect to air, R is the universal gas constant, T is the absolute temperature, ρ_w is the density of water, ρ_s is the density of the dry particle, D_p is the diameter of the aerosol particle (soluble material) as given by the DMA, M_s is the molecular weight of the soluble material, ν is the number of ions into which the soluble molecule dissociates, and ϕ_s is the osmotic coefficient.

The critical drop radius, a_C, is defined as the size of the solution droplet, formed on the aerosol particle, beyond which the droplet is freely growing, i.e., the energy barrier to continued growth has been overcome. a_C is a solution of the equation $dSS/da = 0$, or

$$3BQa^4/(a^3 - r^3)^2 - A - Ba^2Q'/(a^3 - r^3) = 0. \tag{3}$$

Here $Q' = (dQ/dm_0)(dm_0/da)$, where m_0 denotes the molality of the solution droplet. Q can have a weak dependence on molality through the osmotic coefficient. For most materials Q' is sufficiently small to neglect. However in the Results section we will find that some dyes have a sufficiently large Q' to induce a small effect. We first discuss our method for calculating Q when Q' is negligible.

When Q' is taken to be zero, Eq. (3) can be numerically solved for the critical size a_C. A theoretical expression for the critical supersaturation can be generated by inserting a_C into Eq. (2):

$$SS_{C,theor}(D_p, Q) = SS_C(a_C) = A/a_C - BQ/(a_C^3 - r^3). \tag{4}$$

This theoretical expression is a function of D_p and Q. Setting this expression equal to the experimental value of critical supersaturation for a particular value of D_p, yields an equation:

$$SS_{C,exptl} = SS_{C,theor}(D_p, Q), \tag{5}$$

which can be inverted to yield a value of Q for this D_p, i.e., $Q(D_p, SS_{C,exptl})$. This inversion has to be done numerically. Hence each data pair $(D_p, SS_{C,exptl})$ yields a value for Q.

For some dyes Q is found to exhibit a weak dependence on D_p. We attribute this to the fact that the molality of a critical sized drop changes with D_p, and ϕ_s can depend on m_0 (molality). In the following Results section we find that the Q variation can be well fit by the function:

$$Q = z_1 + z_2 \ln(D_p), \tag{6}$$

where z_1 and z_2 are constants for a given material. We can convert this to a molality dependence. The molality (m_0) for a drop of size a containing mass $m_s (= \pi\rho_s D_p^3/6)$ of solute of molecular weight M_s is

$$m_0 = 3000 m_s / 4\pi\rho_w M_s a^3. \tag{7}$$

At critical size, the relation between drop size and solute mass (or D_p) is (Pruppacher and Klett, 1978)

$$\begin{aligned} a &= (3BQ/A)^{1/2} \\ &= (9QM_w m_s/4\pi A\rho_w\rho_s M_s)^{1/2} \\ &= \left(3M_w QD_p^3/8A\rho_w M_s\right)^{1/2}. \end{aligned}$$

Here we drop the Q' contribution to the critical size because we are developing a first-order correction for the variation of Q with m_0. Putting this into Eq. (8) for m_0 yields

$$m_0 = (125\rho_s/M_s) \times \left(8\, A\rho_w^{1/3} M_s/3M_w QD_p\right)^{3/2},$$

which can be inverted to give D_p as a function of m_0:

$$D_p = \left(8A\rho_w^{1/3} M_s/3M_w Q\right) \times (125\rho_s/M_s m_0)^{2/3}.$$

When this is put into the linear relation between Q and $\ln D_p$ we have:

$$Q = z_1 + z_2 \ln\left[\left(8A\rho_w^{1/3} M_s/3M_w Q\right) \times (125\rho_s/M_s m_0)^{2/3}\right], \tag{8}$$

and $dQ/dm_0 = -(2/3)z_2/[m_0(1 + z_2/Q)]$. From Eq. (7) $dm_0/da = -3m_0/a$. Hence

$$\begin{aligned} Q' &= dQ/da = (dQ/dm_0)(dm_0/da) \\ &= 2z_2/[a(1 + z_2/Q)]. \end{aligned}$$

This equation for Q' can be put into Eq. (3) which defines a_C, and then Eq. (5) yields Q. A remaining problem is that one doesn't have a value for z_2 until Eq. (5) is solved for Q for a number of D_p and the functional form, Eq. (6) is fit to the resulting data. However since the Q' contribution is small, this can be handled by iteration. Begin with the assumption that $z_2 = 0$. Find Q at each D_p via Eq. (5). Fit Eq. (6) to this data and get a new z_1 and z_2. Use this z_2 to repeat the process. Repeat until z_2 stops changing. We then have the desired Q for each D_p, and the best fit z_1 and z_2.

Note that this technique provides a way to use cloud chamber critical supersaturation measurements to generate molality dependent values for the osmotic coefficient, provided that ν and ρ_s are known, or for Q alone, which is the parameter needed for hydration information, if they are not known. Given z_1 and z_2, Eq. (8) can be solved numerically, using a nonlinear equation solver or an iterative technique, to give Q or ϕ_S as a function of m_0.

The accuracy to which the above Q determination can be made will depend on the uncertainties in the cloud chamber measurements. For error analysis discussion we put an approximate ($Q' = 0$ and $r = 0$) solu-

TABLE 3. Contributions to Fractional Error in SS_C from Various Sources

SS (%)	8	2	0.32
Voltage	8E-5	9.9E-5	6.8E-4
Flow	0.0144	0.0204	0.0142
Temperature	0.0303	0.0370	0.0572
Thickness	0.04	0.034	0.032
Total	0.0544	0.0655	0.0878

tion to Eq. (3),

$$a_C = (3B/A)^{1/2},$$

into Eq. (4) for the critical supersaturation to find

$$SS_C = (4A^3/27BQ)^{1/2}.$$

This can be inverted to give Q in terms of the measured SS_C,

$$Q = 4A^3/27BSS_C^2.$$

The major uncertainty in Q arises from the experimental uncertainty in SS_C, and the fractional error in Q is simply twice that in SS_C.

The sources of error in determining SS_C arise from several contributions: the central rod voltage and air flow rates in the electric aerosol classifier used to size the aerosol, the temperature on the CFD plates, and the finite thickness of the aerosol stream in the CFD. Table 3 exhibits estimates of the contributions of the various terms to the fractional error in SS_C for various selected supersaturations. The total error is the square root of the sum of the squares of the contributions. Hence our fractional uncertainty in SS_C is about 0.08, and the corresponding uncertainty in Q is twice that, or 16%.

RESULTS

Critical supersaturation data for various fluorescent dye aerosols are shown in Figures 3–6 and 8 and 9. Values of Q were calculated from a subset of this data, i.e., that subset for which SS_C is $< 1\%$. We fit Q to the region $S < 1\%$ so that we can then use this Q to predict the aerosol critical supersaturation for $SS_C > 1\%$ and then compare this prediction with the CFD measurements there. Q was found to be either constant or to have a weak dependence on D_p. The data (Q vs. D_p) can be well represented by the simple function:

$$Q = z_1 + z_2 \ln(D_p).$$

Values for z_1 and z_2 (with D_p given in micrometers) are given in Table 4. Note that for these z values and over the aerosol size range ($0.01 < D_p < 1.0$ μm) studied here, this empirical expression for Q always yields positive values. Physically Q should be positive definite. For most dyes (Figures 3–6) these values were extracted from the critical supersaturation data for $SS_C < 1\%$. Figures 8 and 9 show critical supersaturation vs. size data taken with the CFD for fluorescein 548 and rhodamine 560 chloride, respectively. For these two dyes insufficient data were taken at the larger particle sizes to permit a meaningful $SS_C < 1\%$ analysis. Here we simply fit Q to the entire set of data.

Using values of Q dictated by Table 4 the theoretical expression in Eq. (4) is used to calculate critical supersaturation over the whole range of SS_C, and the results (solid lines) plotted in Figures 3–6 and 8 and 9. The expression is found to fit the experimental data (circles, squares and triangles) very well. The fit is good even at the high supersaturation values, in spite of the fact that the Q information was derived only from the $SS_C < 1\%$ data. There is good continuity between the CFD $SS_C > 1\%$ data,

TABLE 4. Values of M_s, Z_1, and Z_2

Material	M_s	z_1	z_2
Disodium fluorescein	412.31	4.789	0.4228
Sulforhodamine 640	606.72	1.556	0.2306
Sulforhodamine B	558.66	1.450	0
Rhodamine 590 chloride	549.7	1.600	0
Fluorescein 548	426.5	0.6133	−0.1271
Rhodamine 560 chloride	366.8	2.980	0.5214

the CFD $SS_C < 1\%$ data, and the ALGR (high SS_C) data. Critical supersaturations given by Kohler theory using Q parameters fit to the $SS_C < 1\%$ CFD data show good agreement with the high supersaturation data from the CFD and ALGR. The data from Table 4 can be used along with Eqs. (3) and (4) to calculate the critical supersaturation for an aerosol particle in the size range $0.01 < D_p < 0.6$ μm.

CONCLUSION

Several highly pure fluorescent dyes (marketed as the lasing agent for dye lasers) were selected for hydration behavior study. They were used to generate monodispersed aerosols and the critical supersaturation vs. size (SS_C vs. D_p) spectra were measured using the CFD and IT chambers in the supersaturation range ($SS_C < 1.0\%$) where these devices are known to be valid. Using certain operational precautions, the CFD was employed to measure critical supersaturations for these aerosols in the supersaturation region $SS_C > 1.0\%$. The ALGR chamber was used to measure SS_C for SS_C values greater than those accessible to the CFD and for overlapping SS_C values. This SS_C vs. D_p information is presented in Figures 3–6. Data for two other dyes over a more limited size range are shown in Figures 8 and 9. The three instruments are found to give good agreement with each other.

The laser dyes were found to follow Kohler theory in the $SS_C < 1.0\%$ region. A method was developed to use cloud chamber critical supersaturation measurements to generate molality dependent values for an aerosol material's osmotic coefficient. The relevant parameters are given in Table 4. Using this information, their predicted behavior was calculated for the $SS_C > 1.0\%$ region. Their predicted SS_C agreed well with the measured values given by the CFD and the ALGR. The critical supersaturation behavior of these dyes can be interpreted as that of a high molecular weight ionic compound that obeys the Kohler theory. Since the two instruments, ALGR and CFD, agreed with each other and with the predicted Kohler behavior of the aerosols for $SS_C > 1.0\%$, this constitutes the first experimental verification of these instruments in this supersaturation region ($SS_C > 1.0\%$).

This work has been largely supported by the Air Force Office of Scientific Research (AFOSR 85-0071) and by the National Aeronautics and Space Administration (NASA NAS8-34603)

REFERENCES

Alofs, D. J. (1978). *J. Appl. Meteorol.* 17:1286–1297.

Alofs, D. J., and Podzimek, J. (1974). *J. Appl. Meteorol.* 13:511–512.

Alofs, D. J., Trueblood, M. B., White, D. R., and Behr, V. L. (1979). *J. Appl. Meteorol.* 18:1106–1117.

Alofs, D. J., and Trueblood, M. B. (1981). *J. Rech. Atmos.* 15:219–223.

Carstens, J. C. (1979). *Adv. Colloid Interface Sci.* 10:285–314.

Davies, C. N. (1987). *J. Aerosol Sci.* 18:469–477.

Deshler, T. (1982). In *Proceedings* American Meteorology Society Conference on Cloud Physics, Chicago, IL, pp. 111–114.

Elder, J. C., Kyle, T. G., Tillery, M. I., and Ettinger, H. J. (1981). Los Alamos Scientific Laboratory Technical Report LA-8805-MS, NTIS DE81024008.

Gerber, H. E., Hoppel, W. A., and Wojciechowski, T. A. (1977). *J. Atmos. Sci.* 34:1836–1841.

Hagen, D. E. (1979). *J. Appl. Meteorol.* 18:1035–1043.

Hanel, G. (1976). *Adv. Geophys.* 19:73–188.

Hoppel, W. A., Twomey, S., and Wojciechowski, T. A. (1979a). *J. Aerosol Sci.* 10:369–373.

Hoppel, W. A., Twomey, S., and Wojciechowski, T. A. (1979b). *J. Aerosol Sci.* 11:421–422.

Hoppel, W. A., and Wojciechowski, T. A. (1976). *J. Appl. Meteorol.* 15:107–112.

Kohler, H. (1921a). *Meteorol. Z.* 38:168.

Kohler, H. (1921b). *Geofys. Publ.* 2: No. 1.

Kohler, H. (1922). *Geofys. Publ.* 2: No. 6.

Kohler, H. (1927). *Geofys. Publ.* 5: No. 1.

Kohler, H. (1936). *Trans. Faraday Soc.* 32:1152.

Knutson, E. O., and Whitby, K. T. (1975a). *J. Aerosol Sci.* 6:443–451.

Knutson, E. O., and Whitby, K. T. (1975b). *J. Aerosol Sci.* 6:453–460.

Laktionov, A. G. (1972). *Izv. Akad. Nauk. SSSR Fiz. Atmos. Okeana* 8:672–677.

Liu, B. Y. H., and Pui, D. Y. H. (1974a). *J. Aerosol Sci.* 5:465–472.

Liu, B. Y. H., and Pui, D. Y. H. (1974b). *J. Colloid Interface Sci.* 49:305–312.

Mahata, P. C., Alofs, D. J., and Sinnarwalla, A. M. (1973). *J. Appl. Meteor.* 12:1379–1383.

Pruppacher, H. R., and Klett, J. D. (1978). *Microphysics of Clouds and Precipitation*. D. Reidel, Boston, p. 142.

Rowland, J. R., and Konrad, T. G. (1979). Applied Physics Laboratory Technical Report S1R79U-003, Johns Hopkins Univ.

Saxena, V. K., and Carstens, J. C. (1971). *J. Rech. Atmos.* 5:11–23.

Saxena, V. K., and Carstens, J. C. (1971). *J. Rech. Atmos.* 5:11–23.

Sinnarwalla, A. M., and Alofs, D. J. (1973). *J. Appl. Meteorol.* 12:831–835.

Tzeng, H. M., Wall, K. F., Long, M. B., Owen, J. F., and Chang, R. K. (1983). *Aerosol Sci. Technol.* 2:193.

Uthe, E. E., Viezee, W., Morley, B. M., and Ching, J. K. S. (1985). *Bull. Am. Meteorol. Soc.* 66:1255–62.

White, D. R., Kassner, J. L., Carstens, J. C., Hagen, D. E., Schmitt, J. L., Alofs, D. J., Hopkins, A. R., Trueblood, M. B., Alcorn, M. W., and Walker, W. L. (1987). *Rev. Sci. Instrum.* 58:826–34.

Received June 24, 1988; accepted January 17, 1989.